International Journal of Hydrogen Energy 92 (2024) 560–568

Contents lists available at ScienceDirect

International Journal of Hydrogen Energy

journal homepage: www.elsevier.com/locate/he

Catalytic methanol cracking to hydrogen and formaldehyde over heterogeneous catalysts by radiolysis: Sectoral industrial symbiosis by waste radiation utilisation

Anže Prašnikar [a,**], Brigita Hočevar [a], Anže Jazbec [b], Klemen Ambrožič [c], Luka Snoj [c,***], Blaž Likozar [a,*]

[a] Department of Catalysis and Chemical Reaction Engineering, National Institute of Chemistry, Hajdrihova 19, 1001 Ljubljana, Slovenia
[b] Reactor Infrastructure Centre, Jožef Stefan Institute, Jamova 39, 1000, Ljubljana, Slovenia
[c] Reactor Physics Division, Jožef Stefan Institute, Jamova 39, 1000, Ljubljana, Slovenia

ARTICLE INFO

Handling Editor: Dr V Palma

Keywords:
H_2 production
Methanol radiolysis
Sector coupling
Formaldehyde synthesis
Nuclear energy
Waste radiation

ABSTRACT

In order to create a sustainable, carbon-neutral society, it is of utmost importance to link the energy sector with the chemical industry. Radiation from nuclear power plants proves to be useful for H_2 production from water or carriers such as methanol. In our study, we investigated the potential for the production of hydrogen and formaldehyde by endothermic radiolytic cracking of 50 mol% aqueous methanol, which can be produced by direct CO_2 hydrogenation without distillation. We developed an elegant experimental setup and performed irradiation tests in the TRIGA reactor with system analysis by GC-MS (gas chromatography with mass spectroscopy), SEM-EDS (scanning electron microscopy with energy dispersive spectroscopy), XRD (X-ray powder diffraction) and Monte Carlo simulations of radiation absorption. Among the different routes tested, a semiconductor-based photocatalytic material (TiO_2) increased the H_2 yield by 24%. In the critical evaluation of radiation utilisation, spent fuel radiation sources were found to be promising as they require low heat exchange and could produce 3600 kg H_2/day in a single spent fuel pool. The advantage of radiolytic methanol cracking lies in its ability to produce formaldehyde and hydrogen (~53% methanol value increase), whereas conventional partial oxidation of methanol with O_2 for formaldehyde production (only ~31% methanol value increase) inevitably produces water, which reduces the overall energy efficiency.

1. Introduction

The use of hydrogen is becoming increasingly relevant in energy/resource conversion applications. However, its main disadvantages are the difficulties in long-term storage, which generally reduces its economic viability. Methanol is one of the best possible options as it is storable (liquid), can be used for further chemical conversion, and can be produced from CO_2.

In addition, power plant operations will be increasingly intertwined with other energy-intensive industry sectors, such as cement, ceramics, chemicals, etc., where renewables, hydrogen and CO_2 will need to be kept in a circular balance through sectoral industrial symbioses. Accordingly, radiation can be considered useful in nuclear power plants, either for the production of H_2 from water or hydrogen carriers such as methanol.

Traditionally, nuclear power plants have been associated primarily with the production of hydrogen [1]. Correspondingly, work to date has focused primarily on the economics, safety and general technical integration of H_2 production, storage and utilisation at the plant site. Taljan et al. [2], for example, have analysed the integration of wind turbines from an economic perspective. Cerri et al. [3], on the other hand, analysed a plant with a sulphur–iodine cycle and examined the operating costs. In addition, the integration of the Brayton cycle was also investigated by Harvego et al. [4] Avsec et al. [5] carried out a more general benchmarking and compared the economic efficiency with methane steam reforming. An even more comprehensive overview of production

* Corresponding author.
** Corresponding author.
*** Corresponding author.
E-mail addresses: anze.prasnikar@ki.si (A. Prašnikar), luka.snoj@ijs.si (L. Snoj), blaz.likozar@ki.si (B. Likozar).

https://doi.org/10.1016/j.ijhydene.2024.10.204
Received 26 April 2024; Received in revised form 23 August 2024; Accepted 14 October 2024
Available online 25 October 2024

was provided by Fino [6], who considers nuclear energy as just one piece of an energy–hydrogen–carbon puzzle nexus. The methodology for economic evaluation was additionally improved by Antony et al. [7], who focuses on state-of-the-art dual purpose power plant for production of H_2 by electrolysis. In general, this seems to be the most important research direction to date, which also aims to reduce the decrease of water electrolysis costs [8,9]. In addition to economic efficiency, safety appears to be one of the biggest challenges in integration. This was already recognised in 2007 when Nelson et al. [10] developed a probabilistic safety assessment (PSA) for a steam methane reforming plant for H_2 production, linked to a gas-cooled high-temperature nuclear reactor. Especially for large-scale production, safety plays an important role in the transition from blue to green H_2 [11]. Finally, in addition to economics and safety, general technical challenges were also assessed. For example, integration with the thermochemical copper–chlorine cycle [12,13], thermochemical conversion of biomass [14] or electrolysis [15] was evaluated and the prospects analysed.

Irrespective of the assessment of the integration of H_2 production, storage and conversion in nuclear power plants, the utilisation of waste radiation for the splitting of relevant hydrogen carriers, which emerge as the conversion of choice for long-term storage, has so far received little attention. Correspondingly, ammonia, methanol and hydrocarbons still appear to be preferable to the storage of compressed hydrogen for economic and other reasons [16], with the latter two also feeding into the carbon cycle and thus also proving attractive in terms of the sector industrial symbiosis. Radiation could therefore be usefully employed to split methanol in the hydrogen production cycle of integrated carbon capture and utilisation (CCU), taking CO_2 reduction into account. Similar to photocatalysis [17–20], we can use high-energy radiation to drive the reactions at mild temperatures (comparing to thermocatalytic processes), while hydrogen could be produced directly with methanol under high pressure. Nonetheless, this does not appear to have been investigated or evaluated to date.

Regarding the catalytic mechanisms triggered by radiolysis, methanol has so far mainly been considered only as a radical scavenger for hydrogen peroxide, which is oxidised to formaldehyde [21,22]. The only existing study on radiolysis-triggered catalytic reforming essentially introduces the use of TiO_2 [23] and refers to a typical photocatalytic MeOH cracking (9% increase upon addition of TiO_2) [24–27], although no detailed optimisation or evaluation has been performed. Furthermore, the known catalytic materials were not used at all. Water radiolysis received the most attention, where some materials with a band gap between 4 and 6 eV (ZrO_2, Ga_2O_3, …) were identified as active [28].

Thermocatalytic methanol reforming is usually carried out with copper catalyst materials at temperatures above 200 °C and at ambient pressure, as the (extensive) decomposition is thermodynamically favored [29,30]. Although other catalyst materials can also be used, the advantage of supported copper analogues is attractive, as no critical raw material elements are included. Nevertheless, it is important to include them (*e.g.* supported Pt [31]) as a reference, although reactions below 200 °C are slow. We also present the effects of the presence of high-Z elements such as lead and neutron absorption materials such as indium [32]. Pd/In_2O_3 is also an important catalyst material for methanol steam reforming [33] and methanol synthesis [34–36].

The aim of the present research is to evaluate the feasibility of catalytic methanol cracking reactions triggered by γ-radiation and neutron radiolysis. We combine this with known thermal and photocatalysts for hydrogen and formaldehyde production from aqueous methanol solution and other materials that strongly interact with radiation at ambient temperature and pressure. The active phase is identified through detailed material characterisation. The methanol produced by thermocatalytic CO_2 hydrogenation with a mole fraction of 50% could be used directly in this process as a means of long-term hydrogen storage without distillative separation. Additional analyses are provided for a broader sectoral industrial symbiosis relevance/potential.

2. Experimental

2.1. Preparation of materials

TiO_2 P25 (Degussa AG), 5% Pt/SiO_2 (Riogen), $CuO/ZnO/Al_2O_3$ (Hifuel W230, Alfa Aesar) were dried at 110 °C prior to the experiments. ZrO_2 (Sigma) was ground for 4 h in a mixer mill (MM 400, Retsch) using ZrO_2 bearings and dried at 110 °C. 5% Pb/SiO_2 was prepared by incipient wetness impregnation of SiO_2 (Aeroxide 200V, Degussa AG) with an aqueous solution of $Pb(NO_3)_2$ (99.5%, Merck). The volume of the solution was equal to the pore volume of the SiO_2 used. After impregnation, the sample was dried at 110 °C. The 1% Pd/In_2O_3 was prepared by coprecipitation of aqueous solutions of $In(NO_3)_3$ (99.9%) and $Pd(NO_3)_2$ (99.0%, Merck) with a solution of $Na_2CO_3 \times 10H_2O$ (99.0%, Kemika Zagreb) at a pH of 9.2. The precipitate was washed with deionised water, dried and calcined at 573 K for 3 h. A detailed procedure is described in the literature [34].

2.2. Sample preparation

The solid samples were heated to 110 °C to remove the adsorbed compounds on the surface of the materials. Methanol and distilled water were boiled for 5 min to remove dissolved gases and mixed in a 1:1 molar ratio. Preboiled benzene (99.0%, Honeywell) (addition of 1 wt%) is used as internal standard of the liquid phase. The catalyst samples are weighed (200 mg, except for TiO_2–P25 100 mg, for Pd/In_2O_3 50 mg) into the quartz vial (Ultra-high-purity Pur Q, Momentive Technologies) and 2 mL (1.810 g) of the solution is added with the pipette. The vial is purged with He for a few seconds and quickly sealed with silicone/PTFE or butyl rubber caps. We observed that the vial cooled down during the He purge due to the evaporation of $MeOH/H_2O$. We monitored the mass of the liquid, the catalyst material, the quartz vial and the total mass. The solid was dispersed in the mixture for 1 min using an ultrasonic bath. It was found that H_2 and other gases permeate through the butyl rubber caps much slower and provide reliable results.

Preliminary pressure tests of closed quartz vessels with MeOH at higher temperatures (90 °C, total pressure 3.5 bar) showed only 0.7% MeOH weight loss after 11 h under high pressure. When heating to 110 °C (5 bar), the septum was cut at aluminium cap due to septum expansion. If the aluminium cap was modified, the system could also tolerate those conditions without of rupture, while additional significant temperature increase yielded in aluminium cap ejection of the quartz vial. Further information can be found in the Supplementary (Section S4).

2.3. Irradiation

The sample irradiations were carried out in the TRIGA Mark II research reactor of the Jožef Stefan Institute with a maximum steady state power of 250 kW [37–40]. The core configuration is shown in Fig. 1.

All sample sets were irradiated under the same conditions in the triangular channel for 787 s at 250 kW. Therefore, they were exposed to a mixed radiation field, i.e. neutron and gamma radiation. The estimated dose received (KERMA equivalent for human tissue as it the most representative for our samples) corresponds to 37 kGy of gamma radiation and 63 kGy of neutron radiation (100 kGy in total). The dose rates were 47 Gy/s and 80 Gy/s for gamma rays and neutrons respectively. Two samples were irradiated twice as long as usual and therefore received in total 200 kGy (samples denominated HD-high dose). The uncertainty in the exposed doses ranges from 5 to 10%. The latter is a bounding uncertainty.

2.4. Analysis of the samples

After irradiation, the samples were stored for 14 days at low

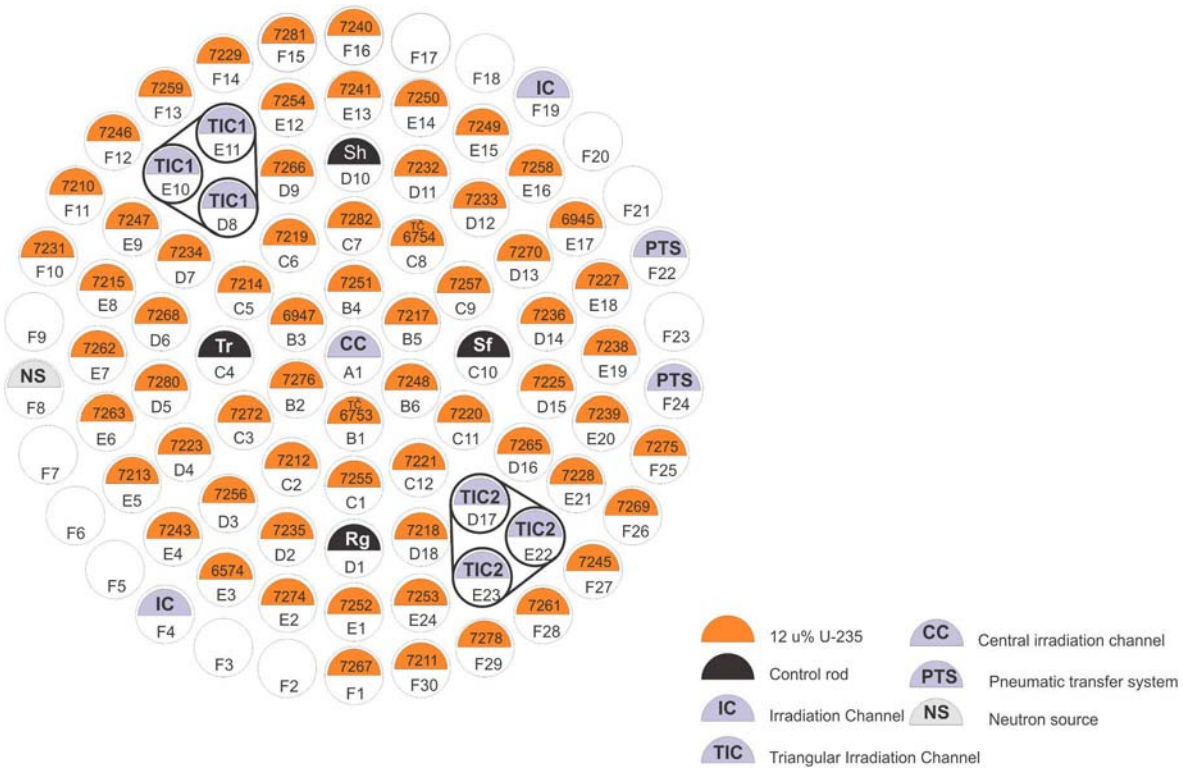

Fig. 1. Core configuration no. 246, which was used for the irradiation of the samples in the triangular irradiation channel 2 (TIC 2).

temperature (−20 °C) in a radiation-protected area to allow the neutron-activated elements (Cu, Ti, Al, etc.) to decay. Once the radioactivity of the samples had fallen below the exemption limit, there was no need to utilize laboratory certified in radioactive material handling for further chemical analyses.

After stabilisation, they were thermostatted to room temperature and weighed. The gas produced was extracted using a syringe. 5 ml of the gas was extracted and diluted to 30 ml using a special Ar purge system to avoid the presence of air. By bending the septum, we found that the pressure in the vials was slightly lower than the ambient pressure, partly due to the filling procedure, where the temperature during vial sealing is lower than the ambient temperature due to evaporation of the solution by the He purge, resulting in a lower amount of He in the closed vial. 5 ml of the gas mixture was analysed three times for each sample by gas chromatography (Agilent 490 Micro GC TCD with CP-COx and PoraPolt U columns) to obtain the concentrations of H_2, He, CO, CO_2 and CH_4 on the COX column (Poraplot U is also used to identify additional products). The liquid product is filtered and analysed by GC-MS (GCMS–QP 2010 Ultra, Shimadzu, Kyoto, Japan) using the Zebron TM ZB–5MSi column to identify formaldehyde, ethylene glycol, MeOH, H_2O, possible additional products, the internal standard benzene and its possible products (cyclohexadiene, anisole, L,4-cyclohexadiene, phenyilcyclohexadiene and biphenyl). For all irradiated samples, we observed no mass loss above 0.009 g. Therefore, we could not detect any significant MeOH/H_2O leakage (max. 0.5%) from the vial.

We monitored the temperature of the CuZnAl sample (dose 100 kGy) by sticking a thin thermocouple to the bottom of the vial. The temperature did not reach 60 °C, as shown in Supplementary (Fig. S6). The temperature increase is largely due to the so-called nuclear heating in the liquid sample [41]. When the irradiation was stopped, the temperature immediately dropped by 1.8 °C, indicating a very small effect of the irradiation on the thermocouple.

The catalysts were characterised using SEM-EDS (scanning electron microscopy with energy dispersive spectroscopy), N_2-physisorption according to the BET theory (Braunauer-Emmett-Teller) and XRD (X-ray powder diffraction) together with Rietveld refinement. The description can be found in Supplementary (Section S1).

2.5. Monte Carlo simulations

The interaction of the incident reactor gamma rays was investigated, particularly with respect to the energy deposited by the induced gamma rays both in pure methanol and in a 10% suspension of TiO_2 in methanol, which could contribute to radiolysis. The simulations were performed using the Monte Carlo particle transport code MCNP v 6.1 [42] and ENDF/B VIII.0 [43] nuclear data libraries. A simplified irradiation setup was simulated, consisting of a 10 m × 2 m × 2 m cube sample with either a uniform, unidirectional surface source at x = 0 or a point source in the centre of the z-y surface, as shown schematically in the Results section. The prompt gamma spectrum taken from previous analyses [44] was considered. The energy deposition was performed in the KERMA approximation, which means that the total energy deposition is considered local (without considering secondary particle transport).

3. Results

3.1. Radiolytic products

The yield of hydrogen gas can be seen in Fig. 2. First of all, we did not observe hydrogen gas either in the control sample (without irradiation) or in the vial filled only with He. Irradiation resulted in an H_2 yield of 2.9 (molecules/100 eV). Based on the extensive H_2 and He permeation tests through the silicone/PTFE septum (Supplementary in Section S2), the H_2 concentration is 29% higher ($G(H_2) = 3.6 \pm 0.1$). The latter tests with butyl septum (not included) showed no significant permeation of gaseous molecules and no correction was needed. In comparison, we found in the literature a yield of H_2 gas of 4.3 for pure γ-irradiation using the same mixture of MeOH and H_2O [45]. We can observe a difference of 5.9% between two samples filled with MeOH solution only. Most of the H_2 (>99%) is in the gas phase, as calculated using Henry's law

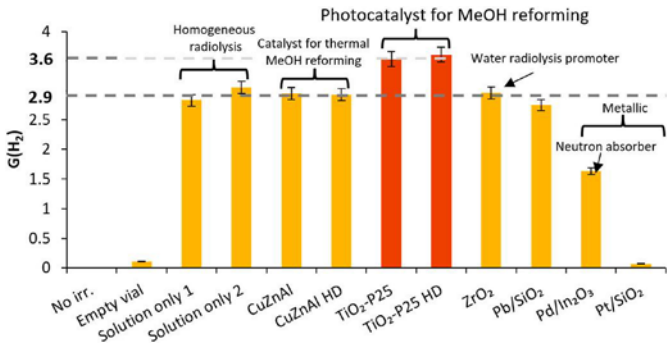

Fig. 2. The H_2 product yield (in H_2 molecules/100 eV) of the samples irradiated with gamma and neutron radiation at an absorbed dose of 100 kGy (HD stands for higher dose - 200 kGy).

(Supplementary, Section S3). The solid sample can influence the H_2 gas yield by increasing or decreasing it. The presence of a CuZnAl sample does no effect on the H_2 yield, while TiO_2–P25 increases it. The metallic samples (Pd- and Pt-based) decreased the H_2 yield, most likely due to the promotion of reactions of H_2 with O_2, which was either formed by H_2O radiolysis, present from the beginning as an impurity, or by the air permeation due to the low pressure in the vessel (Supplementary, Section S2.2). First, we categorised the catalysts into two major groups according to their operating principle: thermal catalysts and photocatalysts. Since TiO_2 is a semiconductor, it obviously promotes methanol cracking through a photocatalytic pathway with γ-rays.

Fig. 3 shows the amount of the main compounds produced (H_2, HCHO, CO and CH_4) as a function of the absorbed dose. It can be seen that an almost linear relationship is achieved for all compounds. The yield of H_2 and HCHO is increased by the presence of TiO_2, while the CO and CH_4 formation remains the same as for the CuZnAl sample (the same as for the MeOH solution only at 100 kGy). Other minor compounds are also present in the gas phase. The most abundant product for the TiO_2–P25 sample is $G(H_2) = 3.6 \pm 0.1$, $G(HCHO) = 2.6 \pm 0.2$, then CO and CH_4 (both 0.17 ± 0.01), followed by CO_2 (0.03), while the yield of ethane and ethene is 0.004 each. Interestingly, we could not detect any ethylene glycol in the liquid phase using GC-MS. The table with all yields can be found in Supplementary (Section S7). In the cases where noble metals were present (Pt/SiO_2 and Pd/In_2O_3), almost all CO was converted to CO_2 and almost all ethene was converted to ethane. As mentioned above, the H_2 yield was also lower in these samples. This could be due to the presence of oxygen in the reaction mixture, the hydrogenation of unsaturated hydrocarbons and due to the presence of

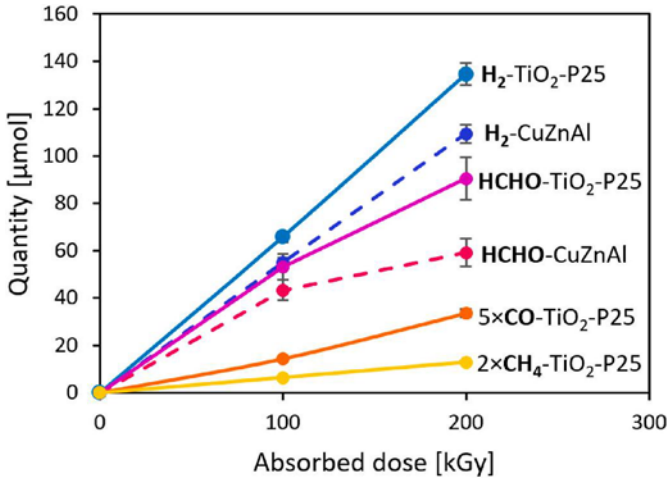

Fig. 3. Ratio between the absorbed dose and the amount of product in the vial produced with 2 mL of a 50 mol% aqueous MeOH solution.

metallic catalyst. No significant increase in HCHO formation was observed with Pt/SiO_2 or Pd/In_2O_3 compared to CuZnAl, suggesting that these catalysts did not promote MeOH radiolysis, although the HCHO yields were much less consistent than the H_2 yields, most likely due to formaldehyde adsorption on solid particles. Overall, TiO_2 promotes the radiolysis of methanol in aqueous solution, forming mainly H_2 in the gas phase and HCHO in the liquid phase.

3.2. Catalyst characterization in relation to the activity tests

The characterisation of the solid material was carried out to determine the structure-activity relationships. The results of the powder X-ray diffraction and N_2-physisorption analyses can be found in Table 1, and all diffractograms with associated peaks and Rietveld refinement fitting, pore volumes and average pore sizes can be found in Supplementary (Section S6). As shown in Fig. 4, only the anatase phase was detected in TiO_2–P25, which is active for photocatalytic MeOH conversion [46], although rutile phase is also active, but high-temperature treatment (700 °C) is required to increase the concentration of surface defects [46]. The crystallite size (d_c) of TiO_2 P25 is 10 nm with a BET surface area of 48.7 m^2/g and SEM average particle size is 19 ± 4 nm, which means that the nanoparticles are highly agglomerated and/or polycrystalline during the N_2-physisorption measurement (theoretical surface area based on an average crystallite size of 140 m^2/g with a TiO_2 density of 4.23 g/cm^3). The adsorption-desorption isotherm of N_2 physisorption can be found in Supporting Information, Fig. S12, and is consistent with microscopy and diffraction findings (low powder (micro)porosity).

The CuZnAl sample used is an unreduced methanol synthesis catalyst and contains precursor phases such as CuO, $Zn_4Al_2CO_3(OH)_{12} \times 3H_2O$ and ZnO, while graphite is added as a binder. Under radiation, metal salt can be reduced to form metal as observed on Au [47] and Cu [48], therefore some structural changes are possible to occur. The ZrO_2 has a relatively small surface area (17 m^2/g) and consists of monoclinic (81%) and tetragonal (19%) phases. It has been shown that tetragonal ZrO_2 can promote H_2O radiolysis with G-values of up to 1.7. Our experiment was performed with a ZrO_2 loading of 10%, while in the reference with similar loading and specific surface area (in the literature 15 m^2/g for the tetragonal sample) the G-value increased from 0.45 for the radiolysis of pure water to 1.1 for the tetragonal sample using γ-rays. A higher tetragonal phase content is therefore likely required to increase water radiolysis using ZrO_2. The absence of a signal due to the presence of the Pb phase in the case of Pb/SiO_2 is an indicator that the Pb phase is finely distributed over amorphous silica. We observed the same phenomenon at 5% Re/C, where no rhenium phase was observed by XRD, where the

Table 1
Results of the analyses of XRD diffractograms and N_2-physisorption.

Sample	Phase name	w [wt. %]	d_c [nm]	BET surface area [m^2/g]
TiO_2–P25	TiO_2-anatase	100	10	49
CuZnAl	CuO-tenorite	49	7	69[a], 93[b]
	$Zn_4Al_2CO_3(OH)_{12} \times 3H_2O$- Zaccagnaite	17	6	
	C-graphite	11	50	
	ZnO-zincite	22.5	2	
ZrO_2	ZrO_2-monoclinic	81	18	17.0
	ZrO_2- tetragonal	19	5	
Pb/SiO_2	Pb (not identified)	5 (nom.[c])	Amorphous or >~5 nm	161
	SiO_2	95 (nom.[c])	Amorphous	
Pt/SiO_2	Pt	5 (nom.[c])	50	154
	SiO_2	95 (nom.[c])	Amorphous	

[a] After reduction in H_2 at 300 °C/12 h [59].
[b] Without reduction [60].
[c] Nominal weight fraction is given.

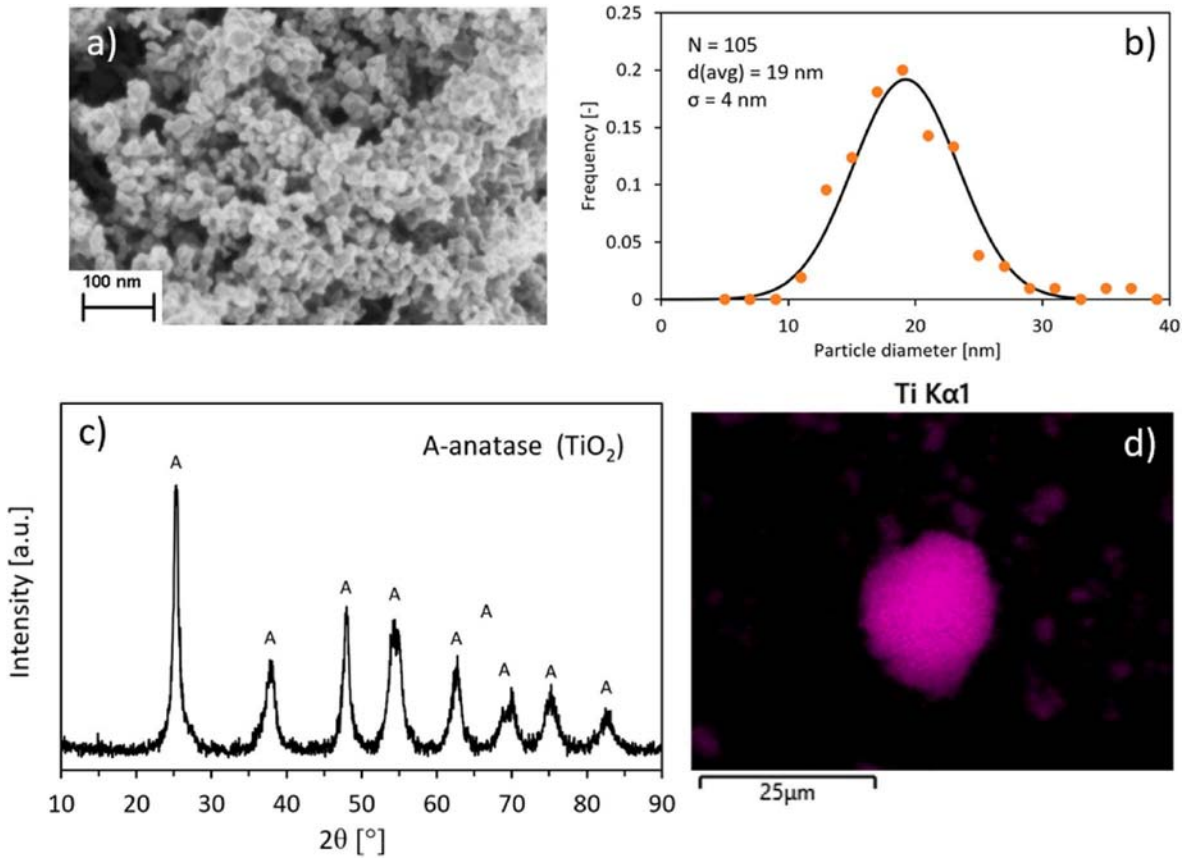

Fig. 4. Characterisation of TiO_2–P25 a) SEM micrograph, b) particle size distribution, c) XRD diffractogram, d) SEM-EDS mapping of agglomerated particles showing only the presence of Ti metal oxide. The Rietveld refinement fit and the diffractograms of the other samples can be found in the Supplementary (Section S6).

average nanoparticle size of 5 nm was determined by TEM [49]. Despite the high interaction with irradiation, the presence of high Z elements (Pb, Pt or Pd) and in the case of Pd/In_2O_3 with indium as neutron absorber [46] did not lead to an increase in methanol conversion based on the yields of H_2 and HCHO (Supplementary, Section S7).

3.3. Influence of the radiation source

The present experiments were carried out using γ- and n-irradiation. The literature shows that the H_2 yield with pure γ-irradiation using a 50% molar aqueous solution of MeOH is equal to 4.2 [45]. The radiolysis of liquid methanol is not only caused by γ-rays or other low linear energy transfer (β) rays. The experiments show similar yields with recoils $^{10}B(n, \alpha)^7Li$, $n+\gamma$, $^4He^+$(3 MeV), 84 MeV recoils ^{235}U or $^{20}Ne^+$ (22 MeV) with H_2 yields ranging from 3.17 to 9.68, while the yields from γ-rays range from 3.46 to 8 [50]. The H_2 product yields of methanol vapour radiolysis in the gas phase are much higher (10–22) [50], but the lower density of the gas phase prevents high volumetric H_2 production.

3.4. Industrial applicability

In this section, we can only consider the aspects related to the tests from our study in the case of a larger H_2 production plant and compare them with the conventional processes. Although Ti is being activated in the presence of neutron radiation, the produced unstable ^{51}Ti has a short halftime of 5.8 min [16,51]. Still, process safety should be thoroughly addressed. In addition, long-term tests should be performed, to identify potential catalyst deactivation issues.

3.4.1. Product purity

Let us first concentrate on the gaseous phase. As a rule, a high purity of H_2 is required for further synthesis or energy conversion in order to achieve stable operation and high efficiency. Let's look at the use of H_2 in fuel cell technology and in the production of NH_3. Stable operation has been reported for NH_3 synthesis with a concentration of 14% of inert materials (CH_4, Ar) in the converter feed with 4.1% purified feedstock [28]. For H_2 fuel cells, no specific effect of the presence of CH_4 has been reported [52], although it reduces activity by dilution similar to N_2 [53]. The presence of CO and CO_2 affects both ammonia synthesis and fuel cell operation. Methanation of carbon oxide residues is usually carried out before ammonia synthesis [54], and the CH_4 produced can be extracted during recycling, which is also typical in H_2 fuel cell operation [55] and methanol synthesis [56].

The current hydrogen concentration is 90.3% (without He) when using TiO_2 and is therefore 0.6% higher than without a photocatalyst. Further improvement of the catalyst would minimise the formation of carbonaceous gases, as TiO_2 only improves H_2 formation among the products in the gas phase. Another possibility is the use of $CH_3\cdot$ scavengers such as halide in the form of dissolved salt ($FeCl_3$) or in elemental form (I_2), which reduces CH_4 formation by 40–65% [57,58], resulting in methyl halides in solution. Changing the pH by adding 0.01 mol/L sulphuric acid could also reduce the CH_4 and CO yields in MeOH by 25% and 20%, respectively. The hydrogen yield can also be increased by 11% by increasing the temperature from 19 °C to 110 °C, which decreases the H_2 solubility, although this would lead to an increase in pressure or evaporation of the solution [50]. Aqueous methanol (50% mol.) can be obtained from the conversion of a CO_2–H_2 mixture and later used for H_2 production without distillation, although MeOH radiolysis is faster than H_2O radiolysis [45], leading to possible H_2O accumulation in the reactor. Besides improving the catalyst, the "greenest" way is to use a water solution of MeOH to reduce CO and CH_4 formation, as roughly illustrated in the work of Seki et al. [45] In addition, a water content of

50% increases the boiling temperature of pure MeOH (from 64 °C to 70 °C at 98 kPa [45]), which allows operation at slightly higher temperatures without the need for high-pressure vessels.

CO and CO_2 could also be converted to CH_4 *in-situ* by using methanation photocatalysts such as Pt/carbon nitride [61], NiO/In_2O_3 and promoted TiO_2, which have been experimentally confirmed to work in the presence of H_2O [62].

For liquid phase circulation it is important that the catalyst is in the form of pellets with a particle size suitable for filtration (in the range of 100 μm [63]). In tests on radiation-induced catalysis, no results were found using catalyst pellets of different sizes, although limiting internal mass transfer could influence H_2 and formaldehyde production.

There are several possibilities for the utilisation of carbon products in the liquid phase. At high MeOH conversion, the solution could be distilled to obtain certain compounds, although tests with high doses need to be performed to identify the products under these conditions. For example, radiolysis of the formaldehyde produced gives ethylene glycol [64] and *vice versa* with possible formation of acetaldehyde [65]. Radiolysis of formaldehyde could also initiate polymerisation to form paraformaldehyde [66]. Alternatively, formaldehyde polymerisation could be chemically initiated to precipitate paraformaldehyde from solution [67]. Formaldehyde is commonly produced by partial oxidation of methanol with O_2 at 300 °C–400 °C. Consuming 35% of the total global methanol produced for this process, formaldehyde is the most important product produced from methanol [68]. Since the partial oxidation route consumes an additional molecule of H_2 for each molecule of formaldehyde and methanol must be distilled to remove water, the process is less energetically favourable than the radiolytic route, where the hydrogen produced (along with CO and CO_2 impurities) could be reused for methanol synthesis as long as waste radiation is used.

3.4.2. Heat balance

Based on the heat capacities of MeOH and H_2O and the applied dose rate of 8.3 kGy/min, we calculated the isothermal temperature rise neglecting the presence of quartz and catalysts. The experimentally measured temperature rise was higher than the isothermal one (by 16%), as can be seen in the Supplement (Fig. S6). The enthalpy of formation of the endothermic reaction of the conversion of methanol to formaldehyde and hydrogen is 85.1 kJ/mol, with a G-value for H_2 formation of 3.6 (MeOH solution with TiO_2), which accounts for 3.2% of the total absorbed energy, and 2.6% for the pure MeOH solution alone. So, the cooling load of the heat exchanger is reduced by the reaction of H_2 formation from MeOH, but as calculated, most of the energy is still converted to heat even if the catalyst is present. However, the energy source is waste ionising radiation, which means that some of the energy is gained.

3.4.3. Scale-up calculations

Waste ionising radiation from PWR (pressurised water reactors) nuclear reactors or spent nuclear fuel could be utilised for H_2 production. However, using an active radiation source only for MeOH radiolysis (instead of electricity production) is currently not economical; only 3.2% of the energy is used for MeOH cracking, and secondly, the combination of heat use from nuclear reactors and heterogeneous catalyst would allow a much better efficiency. At a high dose rate for a nuclear reactor (100 kGy/min), MeOH conversion would be only 0.2%/min at a temperature rise of 32 °C/min (without cooling), giving a H_2 volume productivity of 0.6 mmol (H_2)/L(suspension)/s. For comparison: the steam reforming of methanol using $Cu/ZnO/Al_2O_3$ at 250 °C - 300 °C and ambient pressure results in a volumetric H_2 productivity in the range of 60–220 mmol (H_2)/L (catalyst bed)/s [31]. We have chosen the steam reforming of methanol as a reference and not the partial methanol oxidation, as only this can be used to produce hydrogen. The ratio between heating and activation by radiation is too high for H_2 production from MeOH in the purpose-built nuclear reactor. For this reason, the use of waste radiation with a lower dose rate is much more sensible, as it is difficult to maintain the high temperature for the thermal catalytic conversion of MeOH by radiation and this low-intensity radiation cannot be utilised in any other way. The estimated dose rate for spent fuel source (delayed G) [43] is 604 Gy/h. Given the solution volume that could theoretically be irradiated in an average spent fuel pool of a nuclear power plant (52 m^3), this corresponds to the formation of 3600 kg H_2/day.

Table 2 contains some prices and costs of formaldehyde, methanol and hydrogen. By producing hydrogen and formaldehyde we can increase the value of chemicals (methanol as an input) by around 53%, comparing to conventional value increase of 31% (only formaldehyde production). In the future, hydrogen cost could increase even more if produced by electrolysis and not through steam methane reforming (SMR) coupled with carbon capture and storage (CSS), which will also have an effect on methanol price.

Monte Carlo particle transport simulations of energy deposition were performed to estimate the dimensions of the vessel for radiolytic methanol cleavage. The kerma approximation was validated by the comparison of gamma ray energy deposition (kerma approximation) and energy deposition of electrons, where results are in agreement within their respective uncertainties. The results show that in the case of a surface radiation source (see Fig. 5), the energy deposition in the 10% TiO_2 suspension is initially slightly higher than in the methanol solution, but decreases at a distance of about 30 cm. In the case of a point source (Supplementary, Fig. S13), similar results are obtained, albeit with a less pronounced separation. From this calculation it appears that we harvest 50% of the gamma ray energy in the first ~30 cm and 90% of the energy in ~80 cm of the liquid layer. The final reactor dimensions could be selected on the basis of a more detailed techno-economic analysis. However, one should note that the suspension was simulated as a homogenized material, not as an actual suspension, where electrons stemming from the incident gamma interactions in the TiO_2 could effectively deposit more energy in the solvent, compared to the homogenized material. Such simulations are very computationally intensive, and are beyond the scope of this work.

Fig. 6 shows the hypothetical setup of a MeOH radiolysis process where MeOH is in the liquid phase and the recirculating stream is used for mixing and product removal. Such a plant could be combined with the spent fuel pool or integrated into the side of the PWR. If the desired product is formaldehyde, the gas product (mainly H_2) could be used for methanol synthesis, although the proportion of inert compounds such as CH_4 should be low to avoid accumulation in the recycle loop [56]. In other cases, the process here could also include a COx methanation unit to treat gas for use in fuel cells or in other processes where CO or CO_2 would interfere.

4. Conclusions

The electricity grid and CO_2 management need to be coupled across different sectors to ensure a stable and sustainable system in the long

Table 2
Comparison of the prices of relevant chemicals, identifing that hydrogen price comparing to formaldehyde is substantial.

	Avg. price [$/kg]	Price [$/kmol-pure]	Ref.
Formalin (37%, market price)	0.21	17	[69], methanol price Trend and Forecast, 2022
Methanol (market price)	0.39	13	[69], formaldehyde price Trend and Forecast, 2022
Hydrogen (SMR with CCS, LCOH[a])	1.5	3.0	[70]
Hydrogen (electrolysis, LCOH[a])	5.5	11	[70]

[a] Levelized cost of hydrogen.

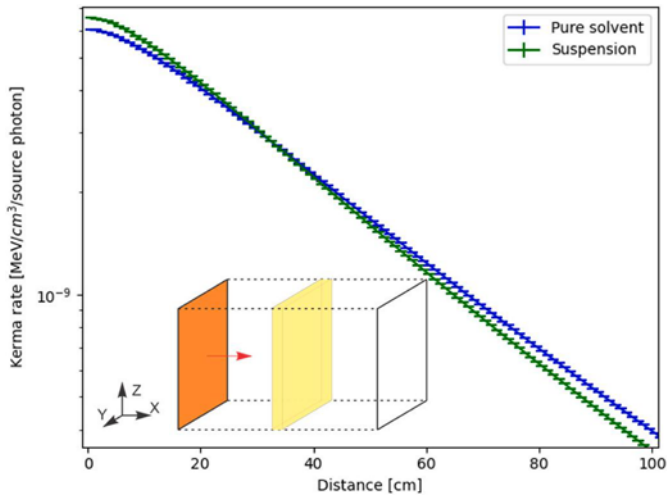

Fig. 5. Surface source gamma ray deposition averaged over the Y-Z plane in pure methanol as solvent and in a 10% TiO_2 suspension as a function of distance from the starting plane in a first meter in X-direction. Uniform surface source (with the source particles in the X-direction. The yellow area marks the tally volume. (For interpretation of the references to colour in this figure legend, the reader is referred to the Web version of this article.)

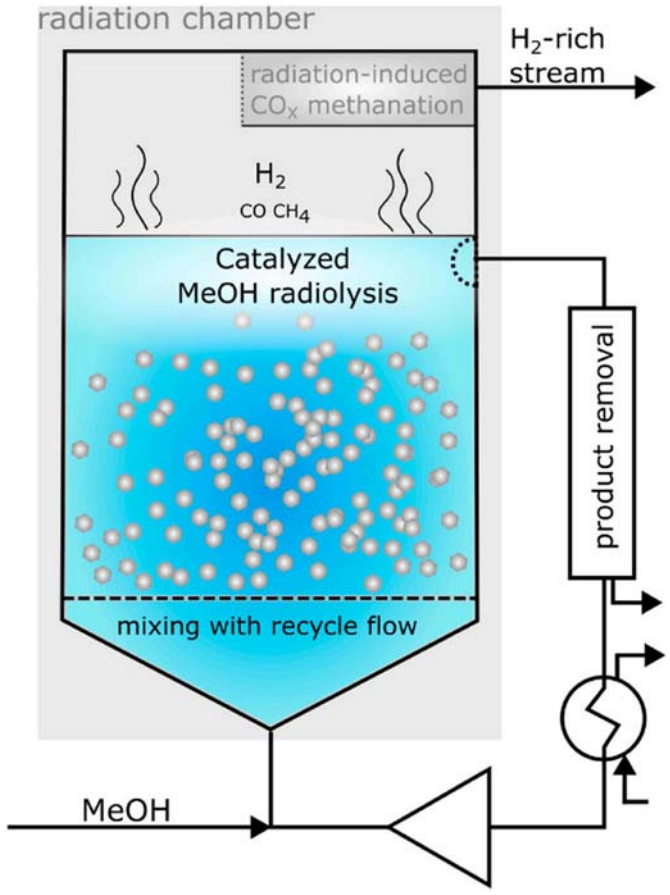

Fig. 6. Radiation-induced process of catalysed radiolytic MeOH cracking with additional pumping system and heat exchanger.

term. Here we have investigated the use of nuclear energy to alleviate the pressure on other sources. In particular, we have assessed the potential for H_2 production and formaldehyde production through endothermic methanol cracking via radiolysis. We found that the semiconductor-based photocatalytic route can increase the yield, with TiO_2 in anatase form increasing the H_2 yield by 24%. A critical review of ionising radiation utilisation was conducted, with the use of the spent nuclear fuel radiation source being the most promising application due to the low heat exchange requirement, although gas purity limits direct H_2 utilisation. An experimental setup with quartz vial, closed by butyl septum was developed to determine the radiolytic activities reliably and efficiently. Interestingly, this radiolytic methanol cracking has an advantage as formaldehyde is conventionally produced by partial methanol oxidation with O_2 in an Ag-based catalyst, producing water instead of valuable H_2. In addition, direct high-pressure H_2 generation may be possible because the reverse reactions with dissolved hydrogen and radical species are less favored in methanol radiolysis compared to water radiolysis, since $G(H_2)$ is about 10 times higher in methanol [71]. Experiments should be performed to determine the change in conversion efficiency when increasing the H_2 pressure.To avoid the use of fossil energy or resources, efficiency must be increased, which is inherently given here by the utilisation of waste radiation for formaldehyde and H_2 production.

CRediT authorship contribution statement

Anže Prašnikar: Writing – review & editing, Writing – original draft, Investigation, Formal analysis, Conceptualization. **Brigita Hočevar:** Writing – review & editing, Investigation, Formal analysis. **Anže Jazbec:** Writing – review & editing, Formal analysis. **Klemen Ambrožič:** Writing – review & editing, Software, Formal analysis. **Luka Snoj:** Writing – review & editing, Supervision, Conceptualization. **Blaž Likozar:** Writing – original draft, Supervision, Funding acquisition, Conceptualization.

Data availability

Data will be made available on request.

Declaration of competing interest

The authors declare that they have no known competing financial interests or personal relationships that could have appeared to influence the work reported in this paper.

Acknowledgments

The research was supported by Slovenian Research Agency on (project UliSess nr. J7-4638, research core funding nr. P2-0152 and project nr. J2-4433). The authors are highly thankful to Ajda Delić for N_2 physisorption measurements and Edi Kranjc for XRD measurements.

Appendix A. Supplementary data

Supplementary data to this article can be found online at https://doi.org/10.1016/j.ijhydene.2024.10.204.

References

[1] Ryazantsev EP, Chabak AF, Ul'yanov AI. Hydrogen production, storage, and use at nuclear power plants, at. Energy 2006;101:876–81. https://doi.org/10.1007/s10512-006-0184-3.
[2] Taljan G, Fowler M, Cañizares C, Verbič G. Hydrogen storage for mixed wind-nuclear power plants in the context of a Hydrogen Economy. Int J Hydrogen Energy 2008;33:4463–75. https://doi.org/10.1016/j.ijhydene.2008.06.040.
[3] Cerri G, Salvini C, Corgnale C, Giovannelli A, De Lorenzo Manzano D, Martinez AO, Le Duigou A, Borgard JM, Mansilla C. Sulfur-Iodine plant for large scale hydrogen production by nuclear power. Int J Hydrogen Energy 2010;35:4002–14. https://doi.org/10.1016/j.ijhydene.2010.01.066.
[4] Harvego EA, McKellar MG, Sohal MS, O'Brien JE, Herring JS. System evaluation and economic analysis of a nuclear reactor powered high-temperature electrolysis hydrogen-production plant. J. Energy Resour. Technol. Trans. ASME 2010;132:210051–9. https://doi.org/10.1115/1.4001566.

[5] Avsec J, Virtič P, Žagar T, Štrubelj L. Economy analysis of electricity production from hydrogen in combination with nuclear power plant. Am. Soc. Mech. Eng. Power Div. POWER 2011;2:345–52. https://doi.org/10.1115/POWER2011-55097.

[6] Fino D. Hydrogen production in conventional, bio-based and nuclear power plants. Woodhead Publishing Limited; 2014. https://doi.org/10.1533/9780857097736.1.85.

[7] Antony A, Maheshwari NK, Rao AR. A generic methodology to evaluate economics of hydrogen production using energy from nuclear power plants. Int J Hydrogen Energy 2017;42:25813–23. https://doi.org/10.1016/j.ijhydene.2017.08.146.

[8] Sorgulu F, Dincer I. Cost evaluation of two potential nuclear power plants for hydrogen production. Int J Hydrogen Energy 2018;43:10522–9. https://doi.org/10.1016/j.ijhydene.2017.10.165.

[9] Marques JGO, Costa AL, Pereira C. Thermodynamic study of a novel trigeneration process of hydrogen, electricity and desalinated water: the case of Na-O-H thermochemical cycle, SCWR nuclear power plant and MED desalination installation. Energy Convers Manag 2020;209:112648. https://doi.org/10.1016/j.enconman.2020.112648.

[10] Nelson PF, Flores A, François JL. A design-phase PSA of a nuclear-powered hydrogen plant. Nucl Eng Des 2007;237:219–29. https://doi.org/10.1016/j.nucengdes.2006.06.006.

[11] Wang K, Zhang X, Miao Y, He B, Wang C. Dispersion and behavior of hydrogen for the safety design of hydrogen production plant attached with nuclear power plant. Int J Hydrogen Energy 2020;45:20250–5. https://doi.org/10.1016/j.ijhydene.2020.04.064.

[12] Dudek M, Jaszczur M, Skolik K, Malicki M, Pieńkowski L. High-Temperature nuclear reactor power plant cycle for hydrogen and electricity production-numerical analysis. E3S Web Conf. 2016;10:1–6. https://doi.org/10.1051/e3sconf/20161000105.

[13] Jianu OA, Naterer GF, Rosen MA. Hydrogen cogeneration with generation IV nuclear power plants. Elsevier Ltd; 2016. https://doi.org/10.1016/B978-0-08-100149-3.00019-7.

[14] Sorokin AP, Alexeev VV, Kuzina JA, Konovalov MA. The problems of using a high-temperature sodium coolant in nuclear power plants for the production of hydrogen and other innovative applications. J. Phys. Conf. Ser. 2017;891. https://doi.org/10.1088/1742-6596/891/1/012086.

[15] Aminov RZ, Bairamov AN. Performance evaluation of hydrogen production based on off-peak electric energy of the nuclear power plant. Int J Hydrogen Energy 2017;42:21617–25. https://doi.org/10.1016/j.ijhydene.2017.07.132.

[16] Akerib DS, Bai X, Bedikian S, Bernard E, Bernstein A, Bradley A, Cahn SB, Carmona-Benitez MC, Carr D, Chapman JJ, Chan Y-D, Clark K, Classen T, Coffey T, Dazeley S, DeViveiros L, Dragowsky M, Druszkiewicz E, Faham CH, Fiorucci S, Gaitskell RJ, Gibson KR, Hall C, Hanhardt M, Holbrook B, Ihm M, Jacobsen RG, Kastens L, Kazkaz K, Lander R, Larsen N, Lee C, Leonard D, Lesko K, Lyashenko A, Malling DC, Mannino R, McKinsey D, Mei D, Mock J, Morii M, Nelson H, Nikkel JA, Pangilinan M, Parker PD, Phelps P, Shutt T, Skulski W, Sorensen P, Spaans J, Stiegler T, Svoboda R, Smith A, Sweany M, Szydagis M, Thomson J, Tripathi M, Verbus JR, Walsh N, Webb R, White JT, Wlasenko M, Wolfs FLH, Woods M, Uvarov S, Zhang C. Radio-assay of titanium samples for the LUX experiment. ArXiv 2011. http://arxiv.org/abs/1112.1376.

[17] Ali SA, Ahmed J, Mao Y, Ahmad T. Symbiotic MoO3-SrTiO3 heterostructured nanocatalysts for sustainable hydrogen energy: combined experimental and theoretical simulations. Langmuir 2023;39:12692–706. https://doi.org/10.1021/acs.langmuir.3c01418.

[18] Ali SA, Ahmad T. Decorating thermodynamically stable (101) facets of TiO2 with MoO3 for multifunctional sustainable hydrogen energy and ammonia gas sensing applications. Inorg Chem 2024;63:304–15. https://doi.org/10.1021/acs.inorgchem.3c03176.

[19] Ali SA, Ahmad T. Enhanced hydrogen generation via overall water splitting using novel MoS2-BN nanoflowers assembled TiO2 ternary heterostructures. Int J Hydrogen Energy 2023;48:22044–59. https://doi.org/10.1016/j.ijhydene.2023.03.118.

[20] Ali SA, Majumdar S, Chowdhury PK, Alhokbany N, Ahmad T. Photoinduced hole trapping in MoSe2-MoS2 nanoflowers/ZnO nanosheets S-scheme conduit for ultrafast charge transfer during hydrogen evolution. ACS Appl Energy Mater 2024;7:2881–95. https://doi.org/10.1021/acsaem.4c00098.

[21] Toijer E, Jonsson M. H2O2 and γ-radiation induced corrosion of 304L stainless steel in aqueous systems. Radiat Phys Chem 2019;159:159–65. https://doi.org/10.1016/j.radphyschem.2019.02.047.

[22] Yang M, Jonsson M. Evaluation of the O2 and pH effects on probes for surface bound hydroxyl radicals. J Phys Chem C 2014;118:7971–9. https://doi.org/10.1021/jp412571p.

[23] Jung J, Jeong HS, Chung HH, Lee MJ, Jin JH, Park KB. Radiocatalytic H2 production with gamma-irradiation and TiO2 catalysts. J Radioanal Nucl Chem 2003;258:543–6. https://doi.org/10.1023/B:JRNC.0000011749.23836.75.

[24] Naldoni A, D'Arienzo M, Altomare M, Marelli M, Scotti R, Morazzoni F, Selli E, Dal Santo V. Pt and Au/TiO2 photocatalysts for methanol reforming: role of metal nanoparticles in tuning charge trapping properties and photoefficiency. Appl Catal B Environ 2013;130–131:239–48. https://doi.org/10.1016/j.apcatb.2012.11.006.

[25] Chiarello GL, Aguirre MH, Selli E. Hydrogen production by photocatalytic steam reforming of methanol on noble metal-modified TiO2. J Catal 2010;273:182–90. https://doi.org/10.1016/j.jcat.2010.05.012.

[26] Šalipur H, Lončarević D, Dostanić J, Likozar B, Prašnikar A, Manojlović D. Nickel-loaded nitrogen-doped titanate nanostructured catalysts for solar-light driven hydrogen evolution and environmental remediation. Int J Hydrogen Energy 2022;47:12937–52. https://doi.org/10.1016/j.ijhydene.2022.02.054.

[27] Šalipur H, Fronczak M, Prašnikar A, Kamal KM, Mudrinić T, Hadnađev-Kostić M, Likozar B, Dostanić J, Lončarević D. Metal doped TiO2 decorated carbon nanostructured materials as an emerging photocatalysts for solar fuels production. Catal Today 2024;436. https://doi.org/10.1016/j.cattod.2024.114724.

[28] Petrik NG, Alexandrov AB, Vall AI. Interracial energy transfer during gamma radiolysis of water on the surface of ZrO2 and some other oxides. J Phys Chem B 2001;105:5935–44. https://doi.org/10.1021/jp004440o.

[29] Palo DR, Dagle RA, Holladay JD. Methanol steam reforming for hydrogen production. Chem. Rev. 2007;107:3992–4021. https://doi.org/10.1021/cr050198b.

[30] Iulianelli A, Ribeirinha P, Mendes A, Basile A. Methanol steam reforming for hydrogen generation via conventional and membrane reactors: a review. Renew Sustain Energy Rev 2014;29:355–68. https://doi.org/10.1016/j.rser.2013.08.032.

[31] Sá S, Silva H, Brandão L, Sousa JM, Mendes A. Catalysts for methanol steam reforming-A review. Appl Catal B Environ 2010;99:43–57. https://doi.org/10.1016/j.apcatb.2010.06.015.

[32] Steinbrück M, Stegmaier U, Grosse M. Experiments on silver-indium-cadmium control rod failure during severe nuclear accidents. Ann Nucl Energy 2017;101:347–58. https://doi.org/10.1016/j.anucene.2016.11.039.

[33] Lorenz H, Turner S, Lebedev OI, Van Tendeloo G, Klötzer B, Rameshan C, Pfaller K, Penner S. Pd-In2O3 interaction due to reduction in hydrogen: consequences for methanol steam reforming. Appl Catal Gen 2010;374:180–8. https://doi.org/10.1016/j.apcata.2009.12.007.

[34] Frei MS, Mondelli C, García-Muelas R, Kley KS, Puértolas B, López N, Safonova OV, Stewart JA, Curulla Ferré D, Pérez-Ramírez J. Atomic-scale engineering of indium oxide promotion by palladium for methanol production via CO2 hydrogenation. Nat Commun 2019;10:1–11. https://doi.org/10.1038/s41467-019-11349-9.

[35] Prašnikar A, Dasireddy VDBC, Likozar B. Scalable combustion synthesis of copper-based perovskite catalysts for CO2 reduction to methanol: reaction structure–activity relationships, kinetics and stability. Chem Eng Sci 2022;250:117423.

[36] Prašnikar A, Jurković DL, Likozar B, Lašič Jurković D, Likozar B. Reaction path analysis of CO2 reduction to methanol through multisite microkinetic modelling over Cu/ZnO/Al2O3 catalysts. Appl Catal B Environ 2021;292:120190. https://doi.org/10.1016/j.apcatb.2021.120190.

[37] Štancar Ž, Snoj L. An improved thermal power calibration method at the TRIGA Mark II research reactor. Nucl Eng Des 2017;325:78–89. https://doi.org/10.1016/j.nucengdes.2017.10.007.

[38] Žerovnik G, Kaiba T, Radulović V, Jazbec A, Rupnik S, Barbot L, Fourmentel D, Snoj L. Validation of the neutron and gamma fields in the JSI TRIGA reactor using in-core fission and ionization chambers. Appl Radiat Isot 2015;96:27–35. https://doi.org/10.1016/j.apradiso.2014.10.026.

[39] Snoj L, Žerovnik G, Trkov A. Computational analysis of irradiation facilities at the JSI TRIGA reactor. Appl Radiat Isot 2012;70:483–8. https://doi.org/10.1016/j.apradiso.2011.11.042.

[40] Štancar Ž, Barbot L, Destouches C, Fourmentel D, Villard JF, Snoj L. Computational validation of the fission rate distribution experimental benchmark at the JSI TRIGA Mark II research reactor using the Monte Carlo method. Ann Nucl Energy 2018;112:94–108. https://doi.org/10.1016/j.anucene.2017.09.039.

[41] Carcreff H, Radulović V, Fourmentel D, Ambrožič K, Destouches C, Snoj L, Thiollay N. Nuclear heating measurements for fusion and fission relevant materials in the JSI TRIGA reactor. Fusion Eng Des 2022;179. https://doi.org/10.1016/j.fusengdes.2022.113136.

[42] Michael R, James MR. LA-UR-13-25911 implementation of cerenkov radiation and reflection/refraction into MCNP6. 2013.

[43] Plant AG, Kos B, Jazbec A, Snoj L, Najdanovic-Visak V, Joyce MJ. Nuclear-driven production of renewable fuel additives from waste organics. Commun Chem 2021;4:1–11. https://doi.org/10.1038/s42004-021-00572-5.

[44] Ambrožič K, Žerovnik G, Snoj L. Computational analysis of the dose rates at JSI TRIGA reactor irradiation facilities. Appl Radiat Isot 2017;130:140–52. https://doi.org/10.1016/j.apradiso.2017.09.022.

[45] Seki H, Nagai R, Imamura M. γ-Radiolysis of a binary mixture of methanol and water. The formation of formaldehyde in the radiolysis of liquid methanol. Bull Chem Soc Jpn 1968;41:1–21. https://doi.org/10.1246/bcsj.41.2877.

[46] LaVerne JA. H 2 formation from the radiolysis of liquid water with zirconia. J Phys Chem B 2005;109:5395–7. https://doi.org/10.1021/jp044167g.

[47] Ambrožič B, Prašnikar A, Hodnik N, Kostevšek N, Likozar B, Rožman KŽ, Šturm S. Controlling the radical-induced redox chemistry inside a liquid-cell TEM. Chem Sci 2019;10:8735–43. https://doi.org/10.1039/c9sc02227a.

[48] Ahmad N, Wang G, Nelayah J, Ricolleau C, Alloyeau D. Driving reversible redox reactions at solid–liquid interfaces with the electron beam of a transmission electron microscope. J. Microsc. 2018;269:127–33. https://doi.org/10.1111/jmi.12568.

[49] Hočevar B, Prašnikar A, Huš M, Grilc M, Likozar B. H2-Free Re-based catalytic dehydroxylation of aldaric acid to muconic and adipic acid esters. Angew. Chemie - Int. Ed. 2021;60:1244–53. https://doi.org/10.1002/anie.202010035.

[50] Baxendale JH, Wardman P. The radiolysis of methanol: product yields, rate constants, and spectroscopic parameters of intermediates. Nsrds-Nbs 1975;54:1–26.

[51] Kim CK, Meinke WW. Thermal neutron-activation analysis of titanium using 5·8-minute titanium-51 and rapid radiochemical separations. Talanta 1963;10:83–9. https://doi.org/10.1016/0039-9140(63)80208-8.

[52] Cheng X, Shi Z, Glass N, Zhang L, Zhang J, Song D, Liu ZS, Wang H, Shen J. A review of PEM hydrogen fuel cell contamination: impacts, mechanisms, and mitigation. J Power Sources 2007;165:739–56. https://doi.org/10.1016/j.jpowsour.2006.12.012.

[53] Boillot M, Bonnet C, Jatroudakis N, Carre P, Didierjean S, Lapicque F. Effect of gas dilution on PEM fuel cell performance and impedance response. Fuel Cell 2006;6:31–7. https://doi.org/10.1002/fuce.200500101.
[54] Smart K. Review of recent progress in green ammonia synthesis. Johnson Matthey Technol. Rev. 2021:230–44. https://doi.org/10.1595/205651322x16334238659301.
[55] Dadvar M, Afshari E. Analysis of design parameters in anodic recirculation system based on ejector technology for PEM fuel cells: a new approach in designing. Int J Hydrogen Energy 2014;39:12061–73. https://doi.org/10.1016/j.ijhydene.2014.06.046.
[56] Prašnikar A, Likozar B. Sulphur poisoning, water vapour and nitrogen dilution effects on copper-based catalyst dynamics, stability and deactivation during CO2 reduction reactions to methanol. React Chem Eng 2022;1073. https://doi.org/10.1039/d1re00486g.
[57] Meshitsuka G, Burton M. Radiolysis of liquid methanol by Co60 gamma-radiation. Radiat Res 1958;8:285–97. https://doi.org/10.2307/3570468.
[58] Adams GE, Baxendale JH. Radical and molecular yields in the γ-irradiation of liquid methanol. J Am Chem Soc 1958;80:4215–9. https://doi.org/10.1021/ja01549a024.
[59] Prašnikar A, Pavlišič A, Ruiz-Zepeda F, Kovač J, Likozar B. Mechanisms of copper-based catalyst deactivation during CO2 reduction to methanol. Ind Eng Chem Res 2019;58:13021–9. https://doi.org/10.1021/acs.iecr.9b01898.
[60] Pori M, Arčon I, Lašič Jurković D, Marinšek M, Dražić G, Likozar B, Crnjak Orel Z. Synthesis of a Cu/ZnO nanocomposite by electroless plating for the catalytic conversion of CO2 to methanol. Catal. Letters 2019;149:1427–39. https://doi.org/10.1007/s10562-019-02717-7.
[61] Shi X, Huang Y, Bo Y, Duan D, Wang Z, Cao J, Zhu G, Ho W, Wang L, Huang T, Xiong Y. Highly selective photocatalytic CO2 methanation with water vapor on single-atom platinum-decorated defective carbon nitride. Angew. Chemie - Int. Ed. 2022;710062. https://doi.org/10.1002/anie.202203063.
[62] Tahir M, Tahir B, Amin NAS, Muhammad A. Photocatalytic CO2 methanation over NiO/In2O3 promoted TiO2 nanocatalysts using H2O and/or H2 reductants. Energy Convers Manag 2016;119:368–78. https://doi.org/10.1016/j.enconman.2016.04.057.
[63] Williams JA, Lefeuvre CW. GB718307A, Improvements in or relating to hydrogenation. 1954.
[64] Novoselov AI, Silaev MM, Bugaenko LT. Dependence of ethanediol yield on formaldehyde concentration in γ-radiolysis of methanol-formaldehyde system at 373–473 K. High Energy Chem 2008;42:69–70. https://doi.org/10.1134/s0018143908010141.
[65] Ahmad M, Awan MH, Mohammad D. γ-Radiolysis of ethylene glycol aqueous solutions. J Chem Soc B Phys Org 1968;7:945–6. https://doi.org/10.1039/J29680000945.
[66] Yamaoka H, Hayashi K, Okamura S. Gamma-ray induced polymerization of formaldehyde, die makromol. Chemie; 1963. p. 196–208.
[67] Brown N. Polymerization of formaldehyde. J Macromol Sci Part A - Chem 1967;1:209–30. https://doi.org/10.1080/10601326708053967.
[68] Heim LE, Konnerth H, Prechtl MHG. Future perspectives for formaldehyde: pathways for reductive synthesis and energy storage. Green Chem 2017;19:2347–55. https://doi.org/10.1039/c6gc03093a.
[69] Huang SY, Huang WE, Yu BY. Rigorous design, techno-economic and environmental analysis of two catalytic transfer hydrogenation (CTH) processes to produce bio-based 2-methylfuran (2-MF). Process Saf. Environ. Prot. 2024;181:429–41. https://doi.org/10.1016/j.psep.2023.11.054.
[70] International Energy Agency, Global Hydrogen Review. Glob. Hydrog. Rev. 2021;2021:223.
[71] Elliot DM, Bartels AJ. Elliot, the reaction set, rate constants and g-values for the simulation of the radiolysis of light water over the range 20° to 350°C based on information available in 2008. Mississauga, Ontario, Ca: Atomic Energy of Canada Ltd.; 2009. Report AECL No. 153-127160-450-001.